# NJC

Accepted Manuscript


This is an *Accepted Manuscript*, which has been through the Royal Society of Chemistry peer review process and has been accepted for publication.

*Accepted Manuscripts* are published online shortly after acceptance, before technical editing, formatting and proof reading. Using this free service, authors can make their results available to the community, in citable form, before we publish the edited article. We will replace this *Accepted Manuscript* with the edited and formatted *Advance Article* as soon as it is available.

You can find more information about *Accepted Manuscripts* in the Information for Authors.

Please note that technical editing may introduce minor changes to the text and/or graphics, which may alter content. The journal's standard Terms & Conditions and the Ethical guidelines still apply. In no event shall the Royal Society of Chemistry be held responsible for any errors or omissions in this *Accepted Manuscript* or any consequences arising from the use of any information it contains.

ROYAL SOCIETY OF CHEMISTRY

www.rsc.org/njc

New Journal of Chemistry

Cite this: DOI: 10.1039/c0xx00000x

www.rsc.org/xxxxxx

RESEARCH ARTICLE

# New emerging rare-earth free yellow emitting 2D BCNO nanophosphor for white light emitting diodes

**Jaya Dwivedi[a], Pawan Kumar[a], Garima Kedawat[b], Bipin Kumar Gupta[a,*]**

***Received (in xxx) Xthxxxxxxxxx 20xx, Accepted Xth xxxxxxxxx 20xx***

**DOI:** 10.1039/b000000x

We have demonstrated a new emerging rare-earth free highly-efficient two dimensional (2D) boron carbon oxynitride (BCNO) yellow emitting nanophosphor with high quantum efficiency for white light emitting diode (WLED) devices. This BCNO nanophosphor exhibits 2D layered structures analogous to hexagonal BN phase. Further, the EELS and XPS results confirm the nanophosphor consisted of B, C, N and O elements. The BCNO nanophosphor has shown a broad highly intense yellow emission band centered at 580 nm corresponding to 470 nm excitation wavelength with a quantum efficiency approaching 89%. This novel nanophosphor with strong emission has subsequently been integrated to chip on board (CoB) based blue LEDs in order to fabricate WLEDs devices with color rendering index of 92. Low color temperature (4899) and better CIE color coordinates (x=0.3496, y=0.3679) of fabricated WLEDs device supports 2D BCNO nanophosphor could be an exceptional choice for CoB based WLEDs. Hence, our method provides a facile synthesis of rare-earth free 2D light weight BCNO nanophosphor and its integration with CoB based blue LEDs for next generation advanced solid state white light applications.

.

## 1. Introduction

Recently, two-dimensional (2D) nanomaterials have been emerging an eminence interest for new access of 2D systems owing to their outstanding physical, chemical, optical as well as structural properties.[1-2] The dimensionality of a material determines its characteristics to a great extent. The discovery of graphene; an atom thick 2D layered structure of graphite, has stimulated tremendous research over 2D materials because of their exotic properties in this regime. These materials have displayed noteworthy potential in arena of electronics devices, optoelectronic devices, van der Waals hetero structures and in various technological applications.[3]

The intensive studies regarding the graphene in recent years marked it as a very intriguing material with astonishing electronic, mechanical and thermal properties, such as high electron mobility and very low resistivity to name a few among others.[1,4-5] However, even after being such an exquisite material, graphene possesses a disadvantage of being sensitive to the ambient so much that its properties can be wrecked by the materials present in proximity. For a system to be able to mimic graphene and yet not entertain alterations in its electronic properties by environment, the material particularly must have a large electronic band gap and no dangling bonds. Consequently, hexagonal boron nitride (h-BN) has drawn considerable attraction of investigators due to its isoelectric resemblance with graphene, which its alternating nitrogen and boron atoms arrangement bear with the atomic arrangement of carbon in graphene. Despite, being structurally similar to graphene, h-BN enjoys the differences, being a wide band-gap semiconductor (~6 eV), high corrosion resistance, better thermal, chemical and mechanical stability, intense UV-emission, high thermal stability and many others.[6-8] The main luminescence peak for pure h-BN was measured at 215 nm (5.77 eV).[9,10] This UV emission is ascribed to the radiative decay of lowest lying exciton called free exciton because it is independent of structural defect of material. However, red shift has been observed due to deep level impurities such as oxygen and carbon.[11,12] The main peak displays several phonon replica on the low energy side due to electron phonon coupling explained by Han et al.[11] who showed that the splitting between the peaks, i.e. the vibrational frequency changes as a function of the boron isotope. Moreover, calculations have also indicated the stability of oxygen in substitution for nitrogen atoms in host BN lattice. The vacancies and other impurities such as carbon could give rise to deep levels as well. To be precise, by controlling the content of carbon and oxygen, it provides an additional way to tune the optical properties. In addition, theories based on quantum chemical calculations predicted that an atomic-level hybridization of h-BN and graphite produce a new semiconducting compound $BNC_x$ with a tunable band gap energy between that of graphite and h-BN depending on

its composition (x) and the atomic configuration in the layer.[13–15] This has a strong impact on potential applications of these materials in hydrogen storage,[12,13] electronic devices,[14,15] electron field-emission,[16] electrocatalysis,[17] as supercapacitor[18] and metal-free phosphors.[19,20] Unfortunately, BCN systems are much harder to synthesize and it is difficult to improve quantum yield of this system, which had only single emission. To date, $BNC_x$ compounds with x varying from 0 to 7 have been prepared by various methods and their photoluminescence (PL) properties have also been investigated.[16-21]

It has been speculated that compounds of $BNC_x$ series may become an appropriate candidate for solid state lightning materials especially for white light emitting diodes (WLEDs). Till date, WLEDs heavily rely on rare-earth doped phosphors (YAG:Ce), which get optically pumped by the emission from blue LEDs.[22] The combined effect of electroluminescence from blue LEDs and photoluminescence of phosphors results in white light. Most of the currently used phosphors in WLEDs are oxides, nitrides, sulfides or oxysulfides doped with rare-earth materials.[23-25] These rare-earth materials are available in meager quantity in nature and, hence, very expensive. Also, their synthesis process requires high temperature and pressure, consequently resulting in large power consumption. Besides, these are heavy metals and their chlorides and oxides are toxic and hazardous for human health as well as for the environment. Hence, the usage of RE-ions phosphors is delimited in the future being economically unfeasible and environmentally harmful. Therefore, a need aroused to prepare phosphors, which are thermally and chemically stable and have non-toxic behaviour, show high luminescence efficiency and have broad excitation and emission spectrum besides being inexpensive. Few of the recently developed phosphors like quantum dots of ZnS:Mn, CdS, CdSe, ZnCuInS/ZnS etc. do not contain rare-earths but still, these materials contain toxic metals like sulfur, cadmium and selenium.[22] Therefore, the development of a novel "yellow" phosphor free from rare-earths as well as toxic metals, which can be synthesized at relatively low temperatures under ambient atmospheric conditions, is desirable for WLEDs applications. A very recent report [I. Akasaki, H.; et. al. doi:10.1038/nphys3147; Nobel Prize awarded on 7th October 2014] for the invention of efficient blue light-emitting diodes, which has enabled bright and energy-saving white light sources could potentially reignite to search out for WLEDs applications in a broad range of layered rare earth free materials.

In light of the above requirements, the present work is explored a new prospect for development of rare-earth free 2D light weight boron carbon oxynitride (BCNO) nanophosphor for WLEDs. In this series, the yellow emitting 2D BCNO nanophosphor has shown a promising future towards this direction to gratify the all desirable properties. Although, few attempts on the synthesis of this material have been explored in details by several research groups, where all of them showing the PL emission of BCNO nanocrystals phosphor[26-29]. However, we attempted the new emerging 2D based BCNO nanophosphor after slight modification in the reported synthesis method.[30,31] The incorporation of oxygen to BCN system has drastically enhanced its color tuning range, which extends from violet to red regions of photoluminescence spectra. The theoretical calculations[21,30] and experimental evidence[19, 31-36] have indicated that tunable visible emission with high quantum yield can be achieved in BCNO compounds, which have metal-free phosphors with low toxicity property. In addition, high external quantum efficiency and a broad range of excitation wavelengths have also been obtained. Very recently, few works on the synthesis of BCNO phosphors using thermal catalytic CVD, solid-state reactions, microwave plasma CVD, a one-step liquid process has been reported with its application being found in the WLEDs.[36,37]

Concisely, in this investigation, we have presented a comprehensive approach towards synthesis of 2D layered BCNO nanophosphor by a facile and low temperature method comparative to known rare-earth based bulk material synthesis.[3] The raw materials used in the synthesis process are readily available and inexpensive such as boric acid, polyethylene glycol (PEG) and urea/carbamide, which makes the overall synthesis process very economical. Moreover, the shape dependent structural/microstructural studies as well as their photoluminescence properties of synthesized nanophosphor have been explored in details. Finally, we have successfully integrated as-synthesized nanophosphor with commercial CoB (chip on board) based blue LEDs for the fabrication of WLEDs.

## 2. Experimental

### 2.1 Synthesis of 2D BCNO nanophosphor

The 2D BCNO nanophosphor was prepared by a facile, inexpensive and customized auto-combustion method. The synthesis process was focused on improving uniform emission with high quantum efficiency. Initially, 0.10 mol of boric acid (boron source, $H_3BO_3$) and 1.00 mol of urea or carbamide (nitrogen source, CO $(NH_2)_2$) were dissolved in 120 gm of ultrapure water. Subsequently, the dispersing agent, polyethylene glycol (PEG, MW-10,000, $H(OCH_2CH_2)_n$ OH) was added to the prepared solution and stirred vigorously at 100°C until a clear transparent aqueous solution was obtained. The chemical structure of boric acid, polyethylene glycol and carbamide are shown in Figure S1 (see supporting information). The XRD patterns of PEG, carbamide and boric acid are given in Figure S2 (see supporting information), which are indexed by JCPDS Card No. 45-0706, 86-2276 and 78-0459, respectively. These clearly demonstrate the presence of their respective pure phases. The resulted solution was heated in closed box type furnace to 400 $^0$C at the rate of 6$^0$C/min and kept at this temperature for 10 min to form pyrolsate (fluffy dry-gel powder form). The closed box furnace was used to control the oxygen during the synthesis process. The pyrolsate step is important in which organic compound is pyrolyzed under condition that would not allow organic compounds to vanish by combustion, so that C/N

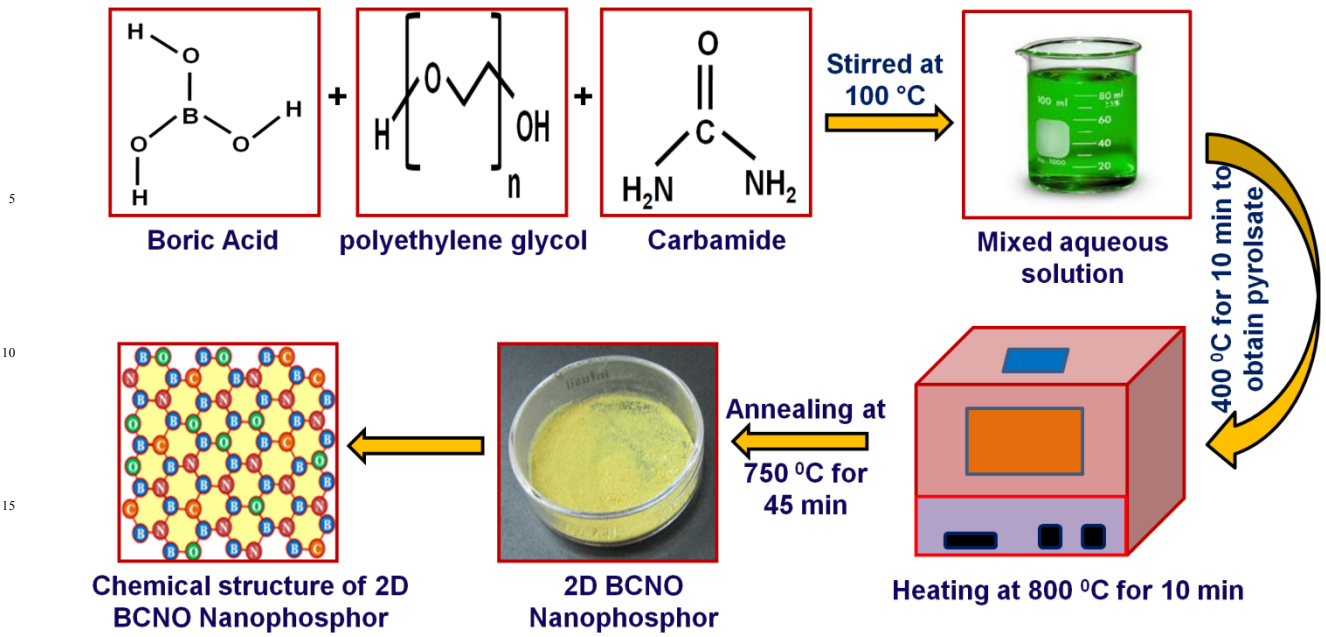


**Fig. 1:** Schematic diagram to synthesize 2D BCNO nanophosphor and its proposed chemical structure with repeated unit cell.

ratio remains constant. The choice of raw material is also quite important for the synthesis of BCNO nanophosphor. The suitability of raw material was decided on the basis of higher photoluminescence intensity of BCNO nanophosphor. We have made several statistical runs with different carbon source such as EG, TEG, PEG 100, PEG 200 and PEG 10,000 to synthesize 2D BCNO nanophosphor for better PL intensity. The PL spectra of various carbon sources based BCNO nanophosphor are shown in Figure S3 (see supporting information). The better result in case of PEG with molecular weight Mw: 10,000 is obtained. Finally, we only focused on PEG as an efficient carbon source to synthesize 2D BCNO nanophosphor. The resulting pyrolsate mixture turned into grey solid due to carbonization of a part of raw material to cause pyrolysis reaction involving deoxidation and dehydrogenation. The pulverized pyrolsate mixture was disintegrated in order to have uniform carbon composition. Then, the mixture was transferred into a ceramic crucible and heated to 800 $^0$C in box furnace at the rate of 25$^0$C/min for 10 min to obtain BCNO precursor. The as-prepared precursor was subsequently annealed at 750 $^0$C for 45 min under the ambient conditions for acquiring the homogeneity throughout the mass. Consequently, a yellow bulk mass was obtained with 86% yield. The schematic diagram to synthesize 2D BCNO nanophosphor and its proposed chemical structure with repeated unit cell is demonstrated in Figure 1. The protocol for the synthesis of 2D BCNO nanophosphor using auto-combustion method is given in Scheme S1 (see supporting information). Here, in this process, the B/N ratio was kept constant, whereas B/C ratio was varied in order to obtain desired wavelength, as shown in Table T1 (see supporting information). It is quite evident that the emission color wavelength can be easily tuned from violet to red regions simply by varying the B/C ratio. As we require yellow nanophosphor for our application point of view, therefore, here, we have only described the synthesis, characterizations and properties of 2D BCNO yellow nanophosphor.

### 2.2 Characterization

The phase purity identification as well as gross structural characterization was performed by XRD technique (Rigaku: MiniFlex, CuK$\alpha_1$; $\lambda$=1.5406Å), which utilizes the principle of Bragg Brantano Geometry. The X-ray scan range starts from 10$^0$ to 80° at a scanning rate of 2° per minute. Prior to the XRD measurement, the diffractometer was calibrated using silicon powder as reference material ($d_{111}$=3.1353Å).[38] The accurate lattice parameters were also obtained through a least square fitting method using computer-based unit cell refinement software.[39] The chemical bonding state was examined with Fourier transformation infrared (FTIR) spectroscopy by NICOLET 6700 instrument using KBr pellets. The spectrum was collected at a resolution of 2 cm$^{-1}$ and each spectrum was an average of 32 scans. The X-ray photoelectron spectroscopy (XPS) analysis was performed in an ultra-high vacuum (UHV) chamber equipped with a hemispherical electron energy analyzer (Perkin Elmer, PHI1257) using non-monochromatized Al K$\alpha$ source (excitation energy of 1486.7 eV) with a base pressure of 4x10$^{-10}$ torr at room temperature. The thickness of 2D layered BCNO nanophosphors was measured by atomic force microscopy (AFM, model: NT-MDT Solver Scanning probe Microscope). Raman spectra were obtained using Renishaw InVia Raman spectrometer, UK with an excitation source of 514.5 nm. The surface morphology and micro-structural characterization were carried out by scanning electron microscopy (SEM, Model No. EVO MA 10 VPSEM) and high resolution transmission electron microscopy (HRTEM, Model No. Technai G20-twin, 200kv with

super twin lenses having point and line resolution of 0.144 nm and 0.232 nm, respectively) equipped with energy dispersive x-ray analysis (EDAX) facilities for elemental studies. The chemical composition of the 2D BCNO nanophosphor was analyzed by electron energy-loss spectrometer (EELS) using a spectrometer attached to the transmission electron microscope. UV-visible spectra were collected using a high resolution UV-vis spectrophotometer (MODEL No.LS 55). Electron paramagnetic resonance (EPR, Bruker A300 EPR) spectrum was collected to give a preliminary explanation of the origin of the fluorescence. The photoluminescence (PL) spectra of nanophosphors were carried out using photoluminescence spectrometer (Edinburgh, FLSP- 920), where Xenon flash lamp acts as source of excitation. Time-resolved spectroscopy was performed by photoluminescence spectrometer with EPL 375 nm picoseconds pulsed diode laser as a source of excitation. In order to estimate the absolute quantum efficiency, we were used an integrating sphere, which is equipped with Edinburgh spectrometer F-900 instrument. The estimation of quantum yield is based on the integrated fraction of luminous flux and radiant flux as per established standard method.[40] The PL mapping was performed by WITech alpha 300R+ Confocal PL microscope system (WITech GnBH, Ulm, Germany), where 375 nm diode laser was used as a source of excitation. The color temperature and CIE color coordinates were measured using colorimeter C1210, serial no. 1296104 and luminance of nanophosphors based WLEDs was calculated by luminance meter series L1000. All the optical photographs were taken from the red sensitive digital CANON PowerShot SX600 HS (16x Megapixels, 5X optical zoom) camera.

## 3. Results and discussion

### 3.1 Structural Analysis

To examine the phase purity, we have performed the XRD of as-synthesized 2D BCNO nanophosphor. The XRD pattern is shown in Figure 2a which indicate the existence of $B_2O_3$, BN and graphitic carbon lattice. It exhibits two broad peaks centered at 26.6° and 41.5° which signifies the formation of hexagonal boron nitride (h-BN; JCPDS no. 74-1978).[41] Besides, there are three more sharp and distinct peaks at 14.5°, 27.7° and 42.8° corresponding to the crystal planes of cubic $B_2O_3$ (JCPDS no. 06-0297). These extraneous peaks are consequence of un-reacted boric acid. The graphitic carbon peak[42] (JCPDS no. 75-1681) at 26.2° appears together with h-BN peak at 26.7°. These peaks are deconvolved by Gaussian fitting, as shown in Figure 2b; the black square mark in Figure 2a exhibits the place where the fitting has been performed. It clearly demonstrates the presence of graphitic carbon, h-BN and $B_2O_3$. The graphene-facilitated formation of h-BN has been observed and these overlapped signals indicate the hexagonal phase of 2D BCNO nanophosphor. The inset of Figure 2b depicts the proposed unit cell of 2D BCNO layers. Each boron atom is surrounded by three nitrogen atoms. Out of which, one of the nitrogen atoms has been replaced by a carbon atom and another one by an oxygen atom to form a BCNO unit cell. These carbon and oxygen atoms behave as an impurity atoms in hexagonal-boron nitride (h-BN) lattice.

A typical FTIR spectrum of as-synthesized 2D BCNO nanophosphor in range of 600-2000 $cm^{-1}$ is shown in Figure 2c. It is clearly justified the 2D nanosheet structure arise in as-synthesized BCNO nanophosphor. The strong absorption bands having centre at ~770 $cm^{-1}$ and ~1420 $cm^{-1}$ unambiguously denote the presence of B-N linkage (stretching mode), which can be attributed to the in-plane and out-of-plane vibration modes of the $sp^2$ hybridized BN.[43,44] The broadening observed in the B-N absorption bands can be ascribed to the incorporation of carbon atoms into host BN lattice.[45]A sharp edge is observed at ~1240 $cm^{-1}$ related to the B-C stretching bond.[36] The two distinctly separate bands observed at ~ 930 $cm^{-1}$ and ~1070 $cm^{-1}$ corresponds to B-N-B bonds and N-B-O bonds, respectively.[47] The vibrational band peaking at ~ 680 $cm^{-1}$ is attributed to the B-O bonds, which are presented in the BCNO nanostructure. Further, the quality of 2D BCNO layer was confirmed through AFM technique. Figure 2d shows a typical AFM image of as-synthesized 2D BCNO nanophosphor, which exhibits a sheet-like nanostructure establishing its 2D structure. The region marked by blue arrows in Figure S4a (see supporting information) exhibits the place, where line-scan profile has been taken to calculate the roughness and thickness of layers. The corresponding line-scan profile indicates a thickness of ~2 nm corresponding to the few h-BN layers, which can be clearly seen in Figure S4b (see supporting information). To ascertain the crystallinity as well as vibration modes of 2D BCNO nanophosphor, we performed Raman spectroscopy, as shown in Figure S5 (see supporting information). It clearly demonstrates the strong peak and oxide phase of BCNO nanophosphor.

Further, the survey-scanned XPS spectrum of as-synthesized 2D BCNO nanophosphor is given in Figure 2e. Prior to the XPS measurement, the calibration of binding energies was done by keeping C1s peak at 284 eV, as standard. The other significant peaks present at 190.27 eV, 397.50 eV and 531.80 eV corresponding to the B1s, N1s and O1s, respectively. The XPS results ensure the formation of BCNO nanocomposite. The XPS core level spectra of B1s, C1s, N1s, O1s, O2s and OKLL region for the 2D BCNO nanophosphor are shown in Figure S6 (see supplementary information). A deep study on the bonding structure of the 2D BCNO nanophosphor was made using XPS B1s, C1s and N1s profiles, which are deconvoluted by Gaussian fitting to get the information about bonding characteristics, as shown in Figures 2f–h. The high-resolution B1s spectrum of the sample (Figure 2(f)) demonstrates three peaks at 190.50, 191.69 and 192.91 eV, which are ascribed to B-O, B-N and B-C bonds, respectively. The high-resolution C1s spectrum (Figure 2(g)) shows four peaks at 283.01, 284.04, 285.43 and 287.05 eV, which are attributed to C-B, C-C, C=C and C-O bonds, respectively. The high-resolution N1s spectrum (Figure 2(h)) reveals three peaks at 397.44, 398.98, 401.04 eV, which are attributed to the pyridinic N, C-B-N and graphitic N bonds, respectively. The above results indicate that the B-N, B-C, B-O

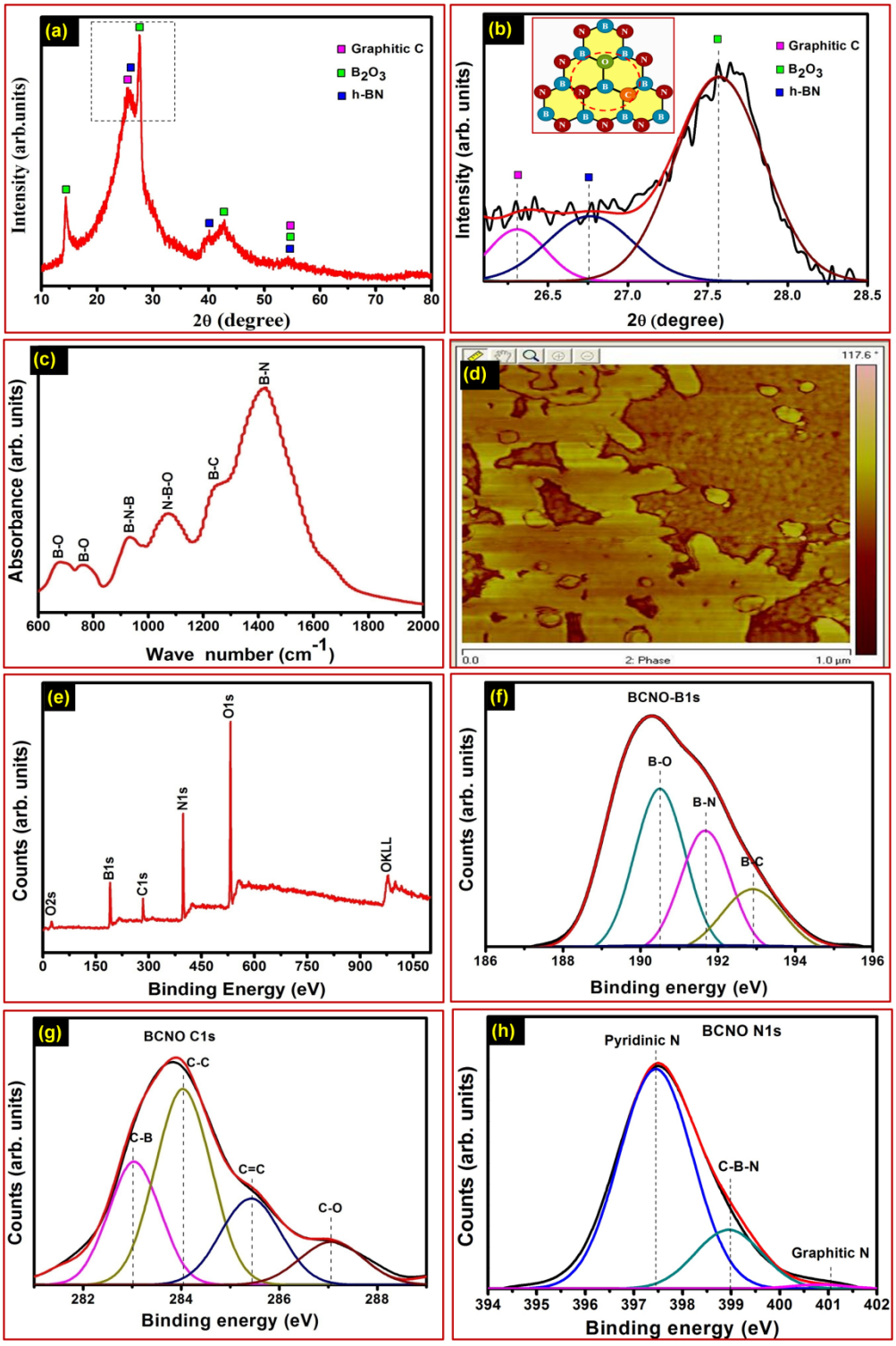


**Fig. 2:** (a) XRD of 2D BCNO nanophosphor, (b) Deconvoluted spectra signifies the formation of hexagonal boron which has been performed from rectangle mark region in Figure 2a, it clearly demonstrate the presence of graphitic carbon, h-BN and $B_2O_3$ and inset exhibits the proposed unit cell of BCNO layered structure, (c) FTIR spectrum of 2D BCNO nanophosphor in range of 600-2000 $cm^{-1}$, (d) AFM micrograph of 2D BCNO nanophosphor, (e) survey-scanned XPS spectrum of 2D BCNO nanophosphor and XPS profile of (f) B1s, (g) C1s and (h) N1s**;** These curves are deconvolved by Gaussian fitting, thereby indicating possible bonding structures.

and C-O bondings are formed in the synthesized 2D BCNO nanophosphor. The basic structure of the sample is the heterocyclic compound unit. The hexagonal phase is also supported by the FTIR spectrum.

**3.2 Surface Morphology and Microstructural Analysis**

To explore the surface morphology and microstructure of 2D BCNO nanophosphor, we have performed SEM and TEM/HRTEM measurements. Prior to SEM and TEM/HRTEM analysis, the BCNO powder samples were sonicated in ethanol using ultra-sonicator operating at 25 kHz frequency to avoid any kind of the agglomerations in the sample consequently leading to better SEM and TEM/HRTEM image quality. Figure 3a represents the SEM image of as-synthesized 2D BCNO nanophosphor. It shows thin 2D randomly oriented layered nanostructure of nanophosphor of irregular shape and having average size of layered sheet ~ 2 μm, which is distinctly visible in the magnified view, as shown in inset of Figure 3a. The TEM image of 2D BCNO nanophosphor is shown in Figure 3b. It signifies that various flakes have combined together to form 2D layered nanostructure, as shown by the yellow marked arrows. The magnified view of TEM image is given in inset of Figure 3b. It also candidly asserts its layered structure with thickness in range of 2 nm. A typical HRTEM image of the specified area marked by red circle in inset of Figure 3b is shown in Figure 3c. The precise observation of HRTEM image indicates the various distinct lattice fringes with different lattice spacing. This signifies that the BCNO nanophosphor is layered in nature and it is composed of few layers. The lattice spacing of the constituent layered nanostructure is 0.34 nm corresponding to the (002) planes of h-BN. The 2D BCNO nanophosphor can also be verified by selected area electron diffraction (SAED) pattern as shown in Figure 3d. The diffraction rings, although somewhat weak due to the stacking of few layers, can be distinctly assigned to the (002), (100), (004), and (110) planes of h-BN (JCPDS no. 73-2095). Figure 3e is the EDAX spectrum of 2D BCNO nanophosphor, the marked by red circle in Figure 3b exhibits the place where EDAX spectrum has been taken. The elements detected by EDAX are largely comprised of B, C, N, and O with mass fractions of 0.13, 0.75, 0.07, and 0.04, respectively. This result was consistent with the composition of the precursor used in the experiment. The chemical composition of the BCNO nanophosphor was further analyzed using an electron energy-loss spectrometer (EELS), which measures the energy imparted to a thin (~200 nm) specimen by fast (~100 keV) incident electrons, from which high spatial resolution of chemical information can be gained. The EELS spectrum is shown in Figure 3f. It exhibits two sharp peaks of B–K ionization at 193 and 201 eV for π* and σ* electrons, respectively. As Garvie et al. pointed out, in the case of a BCNO compound, if the B–K ionization for π* electrons has three peaks of 189.3, 192.1, and194.1 eV, the B atom is surrounded by three elements, i.e., C, N, and O, respectively. Since the B–K ionization for π* electrons had only one peak between 192 and 194 eV, this meant that the B atom was intermediately surrounded by N and O atoms, which also implied that there were no clear B–C chemical bonds in the BCNO compound. The peak at 285 eV is assigned to π* bands, while at 288 and 295 eV are classified as σ* bands, in which the peak at 288 eV has C–H* features. Previous research showed that materials with weak $sp^2$ hybrid orbitals, such as amorphous carbon, graphite, and solid benzene, can have a π* feature; while those having stronger $sp^3$ hybridization[13], such as a diamond and solid cyclohexane, exhibit only σ* (including C–H*) features with no π* bands. The C–H* feature can usually be found in organic materials, such as solid benzene and cyclohexane. In the present study, the C–H bonds are supposed to come from the organic residue of decomposed PEG. Since these data are evidence that the C atoms in the BCNO nanophosphor has π and σ bonds, they should have $sp^2$ hybridization. The $sp^2$ hybrids lie in a plane and are oriented toward the corners of an equilateral triangle at angles of $120^0$ to one another and have a framework consisting mainly of a 6-membered carbon ring. Previously reported EELS data of C–K edges from different carbon sources supported the above hypothesis that the carbon in the BCNO compound has an amorphous structure with traces of C–H groups (organic residue). These should not have a $sp^3$ structure that is rigid and hard, which can be obtained only under extreme conditions. In the present investigations, the BCNO compounds were prepared at low temperature (below 900 ºC) and under ambient atmospheric conditions, resulting in a powder with a soft framework ($sp^2$ hybridization). The ionization peak of N for the π* character is at 403.5 eV and the σ* character at 410.5 eV. Since the σ* peak intensity of N is higher than that of the π* peak, this means the major N atoms have σ* bonds with other elements. The ionization peak spectrum of O is also shown in Figure 3f, where the peaks at 537 and 545 eV are for the π* and σ* character, respectively. Basically, BCNO phosphor is covalently bonded (with π* and σ* bands) to the B and O atoms with a soft ($sp^2$ hybridization) carbon lattice. The structure has been proposed on the basis of the deconvolution core level XPS spectra of B1s and C1s, where clearly B-C, B-O, B-N bonds and C-B, C-C, C=C and C-O bonds are appeared in the proposed structure (inset of Figure 2b) which is also legitimated by EELS results. The obtained EELS data have good consistency with XRD and FTIR results.

In order to understand the presence of delocalized π electrons on the surface of BCNO and carbon contained impurity and their important role in luminescence process, we have performed electron paramagnetic resonance (EPR) studies. The EPR spectrum was recorded at the frequency 9.866 GHz under room temperature. The EPR spectrum of 2D BCNO nanophosphor is shown in Figure S7 (see supporting information). It reveals that the origin of EPR signal for h-BN can been assigned to paramagnetic centers of electrons trapped in the nitrogen vacancies of two different types: three boron center and one boron center. Furthermore, Zunger and Katzir, Anderi et al, and Adobe et al. clarified, based on experimental results as well as quantum chemical calculations that there exist a close relationship between the formation of paramagnetic center (nitrogen vacancy) and impurity of carbon, which produces luminescence centers with an energy level of ~4.1 eV. In present BCNO investigation, we can interpret it as a carbon doped hexagonal compound of BNO. The origin of the emission band is also assumed to be released to the impurity level of carbon. The g-factor is estimated to be ~2.00019 ±0.00004.

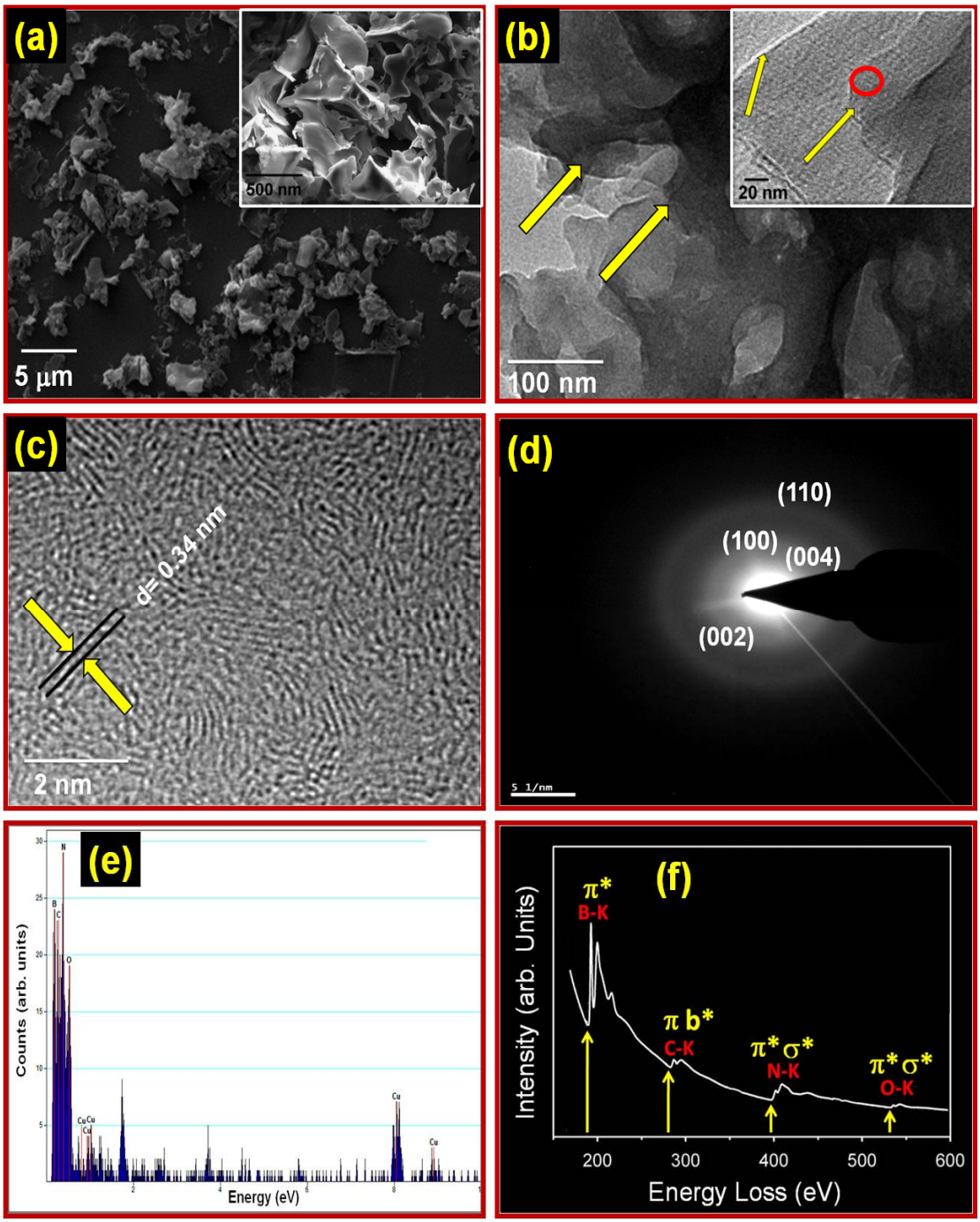


**Fig. 3:**(a) SEM image of 2D BCNO nanophosphor; inset shows its magnified view clearly demonstrating the 2D layered structure, (b) TEM image of 2D BCNO nanophosphor; inset shows magnified view of area marked by yellow arrow in Figure 3b, (c) HRTEM image of 2D BCNO nanophosphor; the image has been taken at the specific area marked by red circle in inset of Figure 3b, (d) SAED of 2D BCNO nanophosphor, (e) EDAX spectrum of 2D BCNO phosphor and (f) EELS spectrum of 2D BCNO nanophosphor.

### 3.3 Optical Spectroscopy Analysis

The UV-Vis absorption spectrum of 2D BCNO nanophosphor is shown in Figure S8 (see supporting information). The sample was dispersed in DI water and sonicated for 2 hours before taking the spectrum. The absorption spectrum reveals narrow and broad peaks at ~231 and ~293 nm, respectively. The narrow absorption peak is probably induced by the absorption of valance band electrons, while the wide absorption peak might be originated from the absorption of carbon related defects. The observed absorption spectrum data is in good correlation with observed photoluminescence (PL) results, which is further discussed in next section.

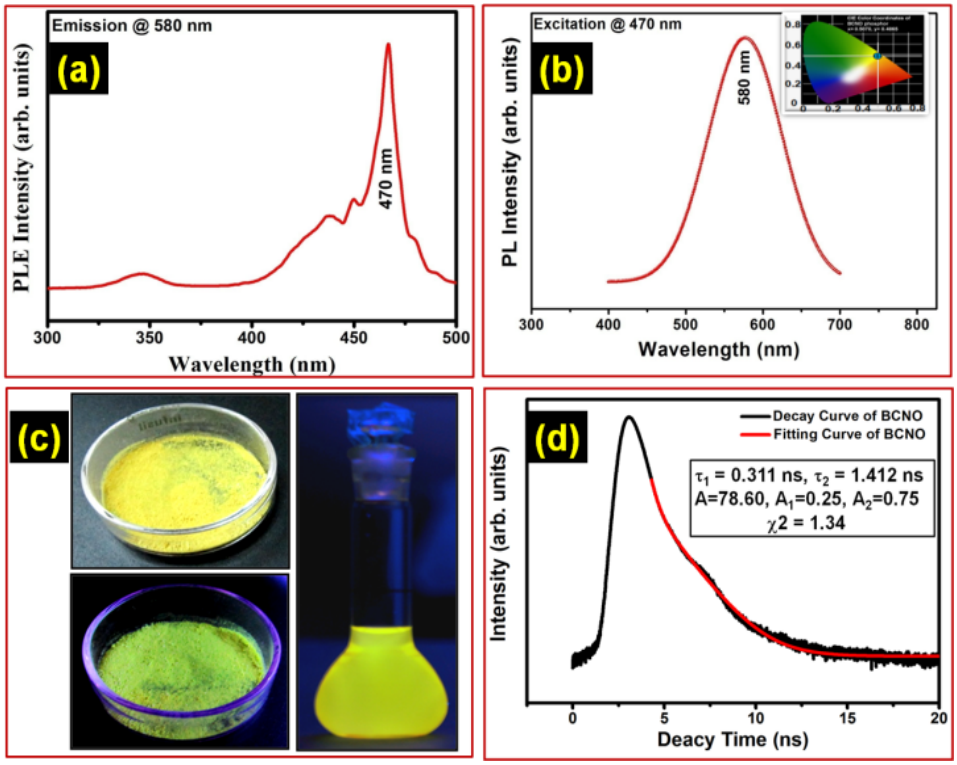


**Fig. 4:** (a) excitation spectrum of 2D BCNO nanophosphor at 580 nm emission wavelength, (b) emission spectrum of 2D BCNO nanophosphor at 470 nm excitation; inset shows the CIE coordinates from emission spectra of 2D BCNO nanophosphor, (c) Top Figure exhibits the powder under normal light with yellow body color, while the bottom powder exhibits yellow color under 340 nm UV lamp and right side bottle shows strong yellow color emission of dispersed BCNO powder in DI water when exposed to 340 nm UV lamp and (d) time-resolved photoluminescence decay spectra with fitting curve and their corresponding parameters of 2D BCNO nanophosphor.

The main aim of the present work is related to fabrication of yellow nanophosphor based white light CoBs. We have tailored the PL emission of 2D BCNO nanophosphor via fixing the B/N ratio and tailoring the B/C ratio. The various concentrations of B/C ranging from 25/0 to 25/0.3 (A = 25/0, B = 25/0.05, C = 25/0.10, D = 25/0.15, E = 25/0.20,F = 25/0.25 and G = 25/0.3) are varied accodingly, subsequently leading to different color emitting BCNO nanophosphor as shown in Figure S9 (see supporting information) and summarized data are given in Table T1 (see supporting information). The role of the carbon atoms in the 2D BCNO nanophosphor plays an key role in the tailoring of band gap, which accompanies the changes in the color emission in BCNO nanophosphor.[36] The optical photograph of 2D BCNO nanophosphor dispersed in water under room light and same phsophors under 340 nm (portable UV lamp) excitation wavelength are shown in Figure S10a and 10b (see supporting information), respectively. Therefore, the suitable value of time, concentration, ratio of B/C and temperature are found to be optimum value for the synthesis of yellow 2D BCNO nanophosphor for WLEDs applications.

The PLE spectrum of 2D BCNO nanophosphor under 580 nm emission wavelength is shown in Figure 4a. We also performed the photo-beaching experiment of 2D BCNO nanophosphor. The obtained result reveals that nanophosphor exhibits better stability of PL as shown in Figure S11 (see supporting information).

Figure 4b represents the emission spectra of yellow emitting 2D BCNO nanophosphor at 470 nm excitation wavelength. The probable two PL mechanism proposed till date on BCNO nanophosphor are as follows: (i) one possible mechanism is that the emission of BCNO nanophosphor may be introduced by the core shell $BO^-$ and $BO_2^-$ anions acting as luminescent centers[35] ($^2\pi_g \rightarrow {}^1\Sigma^+_g$) and (ii) The other possible mechanism can be attributed to impurity defects specially nitrogen vacancies in BCNO nanophosphor. The CIE color co-ordinates (chromaticity diagram) obtained from emission spectra are x = 0.5070 and y = 0.4865, as shown in inset of Figure 4b. It is located typically in the yellow region. Figure 4c represents the synthesized 2D BCNO nanophosphor powder, top one exhibits the powder under room light with yellow body color, while the bottom powder indicate yellow emission under 340 nm UV lamp and in right side, round flask shows strong yellow color emission of dispersed BCNO powder in DI water, when exposed to 340 nm UV lamp.

On the basis of obtained PL results, a simple proposed energy level diagram is tentatively constructed to explain the spectral properties of 2D BCNO nanophosphor, as shown in Figure S12 (see supporting information). The carbon impurity levels are 4.1 eV below the conduction band, while the nitrogen vacancy levels are 0.7–1.0 eV below the conduction band. The excitation at 280 nm (4.4 eV) is probably induced by the transition from the valence band to nitrogen vacancy level and the excitation at 340

nm (3.4 eV) is likely due to the transition from carbon impurity levels to nitrogen vacancy levels. The other long wavelength excitation peaks are probably originated from the carbon related defects to nitrogen vacancy levels; the carbon related defects included substitutional CB and CN defects (whose levels are about 2.2 eV below nitrogen vacancy levels) and interstitial carbon (whose levels are about 1.7 eV below nitrogen vacancy levels), which has been reported to generate deep levels below the conduction band in the range of 2–4 eV. The estimated external quantum efficiency (EQE) of the 2D yellow emitting BCNO nanophosphor is as high as 89%, compared to some rare earth YAG:Ce for WLEDs applications.[22] Time-resolved photoluminescence (TRPL) was recorded using a time-correlated single photon counting technique, using a 375 nm EPL pulse diode laser as a source of excitation. The time-resolved photoluminescence decay spectra with fitting curve and their corresponding parameters for 2D BCNO nanophosphor are shown in Figure 4d. The PL decay was recorded for 580 nm emission at 375 nm excitation wavelength. For BCNO nanophosphor, the decay time is in the range of nanoseconds. Since, excitation lifetime is a size dependent parameter, smaller the size of the nanophosphor, the shorter would be the excitation lifetime and higher would be its recombination rate. The lifetime data of 2D BCNO nanophosphor transitions are very well fitted to a double-exponential function as described by the equation

$$I(t)=A_1\exp(-t/\tau_1)+A_2\exp(-t/\tau_2) \quad (1)$$

Where $\tau_1$ and $\tau_2$ are the decay lifetimes of the luminescence, and $A_1$ and $A_2$ are the weighting parameters. The observed lifetimes for BCNO nanophosphor are $\tau_1 \sim 0.311$ ns and $\tau_2 \sim 1.412$ ns. In 2D BCNO nanophosphor, there are many defects such as N vacancy, substitutional defects (CB or CN) and B/O-related defects in the crystalline parts as well as near crystalline sites in the amorphous parts and these defects would generates different defect levels and affect the fluorescent lifetime. The obtained lifetime results have shown second order exponential decay, which is consistent with earlier reported paper on BCNO nanophosphor.[47] However, the value of the decay components depends upon the quality, composition, intrinsic and extrinsic parameters of the material. For double-exponential decay, the average lifetime ($\tau_{av}$) is determined by the following equation.

$$\tau_{av}=(A_1\tau^2_1+A_2\tau^2_2)/(A_1\tau_1+A_2\tau_2) \quad (2)$$

The average lifetime for BCNO nanophosphor is calculated to be $\tau_{av} \sim 0.4$ ns.

3.4 Fabrication and characterization of CoB based WLEDs

For the fabrication of WLEDs, the as synthesized yellow 2D BCNO nanophosphor was dispersed in epoxy resin with curing agent. A solvent exchange process was developed to disperse the 2D BCNO nanophosphor in an epoxy resin with appropriate amount. We have tried several polymer such as silicon, poly methylmethacrylate (PMMA), epoxy and polycarbonate (PC) in which we have chosen epoxy resin owing to its higher refractive index (1.5), so as to decrease the total internal reflection. Initially, 2D BCNO nanophosphor of 20 mg was dispersed in an epoxy solution (mixture of epoxy resin and a curing agent which acts as a hardener). A spray set-up was used for coating the solution of 2D BCNO nanophosphor on CoB based blue LEDs. The ratio of epoxy resin and hardener was taken to be 100:12.5 by volume. The above mixture was uniformly mixed to make homogeneous mixture. After that, it was carefully spray coated on CoB based blue LEDs arrays (LED FLOOD LIGHT Outdoor display light; 10W power, 120° beaming angle, DC 12 V`, InGaN based ROHS, ISO 9001 registered company, made in China). Afterwards, it was left without further treatment to get dried at room temperature for few hours before testing. The detailed fabrication protocol of CoB based WLEDs from the as synthesized 2D BCNO nanophosphor integrated to CoB based blue LEDs is shown in scheme S2 (see supporting information).

Prior to the fabrication of the 2D BCNO nanophosphor integrated to CoB based blue LEDs, we have performed the PL experiment at different temperature to explore the PL stability (thermal quenching effect), as shown in Figure S13 (see supporting information). The obtained results clearly demonstrate that this 2D BCNO nanophosphor is highly stable at all the performed temperature (room temperature, 50, 100, 150, 200 and 250 °C. The experiment was specially performed upto 250° C because it is likely that the heat dissipation from the CoB based blue LEDs arrays may be generate the temperature upto 200° C.

Figure 5a and 5b shows the uncoated CoB based blue LEDs arrays and 2D BCNO nanophosphor coated CoB based blue LEDs arrays, respectively. To examine the homogeneity of nanophosphor coating on blue CoB based LED, we have performed PL mapping of nanophosphor coated area. Figure 5c exhibits uniform distribution of nanophosphor throughout the surface of chip and inset shows the clear view of uniform coating and black cross mark presents the selected area where PL mapping has been performed. The confocal microscope during the process of PL mapping is given in Figure S14 (see supporting information). Figure 5d reveals the electroluminescence (EL) emission spectrum of commercial CoB based blue LEDs glowing on 12 volt DC power supply. The EL emission spectrum of blue LED significantly overlaps with excitation spectra of nanophosphor, as shown in Figure 4a, which implies its suitability for pumping yellow nanophosphor. Figure 5e presents the EL spectrum of commercial CoB based blue LEDs coated with as synthesized 2D BCNO nanophosphor glowing at different (9,10,11,12) volt DC power supply. It reveals the blue to white light conversion with high efficiency through the yellow BCNO nanophosphor at 12 volt power supply and efficiency decreases when goes down to lower voltage. The inset of Figure 5d and 5e show the optical image of CoB based blue LEDs before and after 2D BCNO nanophosphor coating, respectively, in the glowing mode. The electroluminescence measurement instrument along with yellow nanophosphor coated CoB based LEDs is shown in Figure S15 (see supporting information). The color temperature

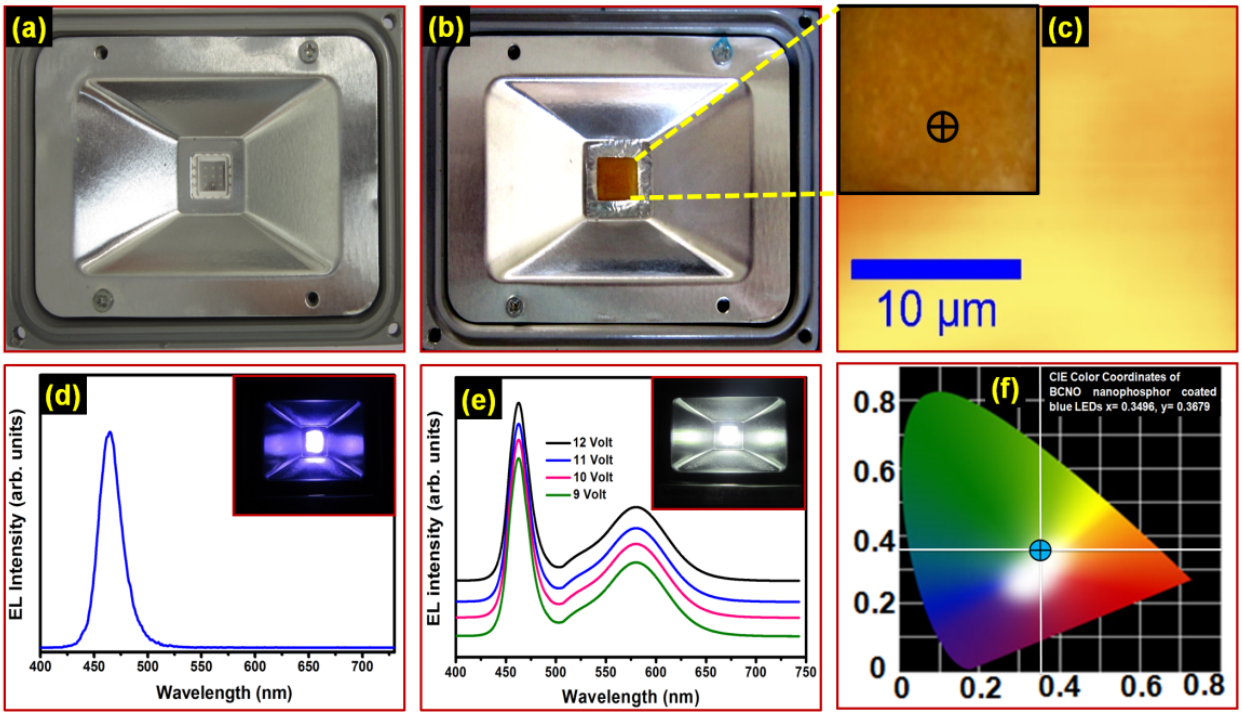


**Fig. 5:** (a) uncoated CoB based blue LEDs arrays, (b) 2D BCNO nanophosphor coated CoB based blue LEDs arrays, (c) PL mapping of 2D BCNO nanophosphor coated blue CoB based blue LEDs; inset shows the clear view of uniform coating and black cross mark presents the selected area where PL mapping has been performed, (d) EL emission spectrum of commercial CoB based blue LEDs without phosphor coating at 12 volt DC; inset shows the optical image of CoB based blue LEDs in the glowing mode, (e) white light EL emission spectrum of fabricated nanophosphor coated blue CoB based LEDs at 12 different voltage (9, 10, 11 and 12 Volt) DC power supply; inset shows the optical image of 2D BCNO yellow nanophosphor coated CoB based blue LEDs in the glowing mode and (f) CIE color co-ordinates of 2D BCNO yellow nanophosphor coated CoB based blue LEDs.

and CIE color co-ordinates measurement instrument is shown in Figure S16 (see supporting information). The CIE color co-ordinates of BCNO yellow nanophosphor coated CoB based blue LED is shown in Figure 5f. It is quite evident from this Figure that emission of BCNO yellow nanophosphor coated CoB lies considerably in the white region having color co-ordinates x = 0.3496 and y = 0.3679. Thus, the obtained excellent results (color rendering index~92, color temperature ~4899 K, luminous efficiency ~83.4 $lmW^{-1}$ and brightness 834 $Cd/m^2$ (the brightness of the device 2D BCNO yellow nanophosphor coated CoB based blue LEDs has been also tested for different time interval to know the feasibility of the device, as shown in Table T2 (see supporting information)) with external quantum efficiency of 2D BCNO nanophosphor coated CoB based blue LEDs arrays ~73%) of this 2D emerging BCNO nanophosphor legitimate its potential applications in next generation rare-earth free 2D light weight material based WLED devices.

## 4. Conclusions

In summary, we have successfully synthesized light weight, rare-earth free 2D BCNO (boron carbon oxynitride) nanophosphor by a facile customized auto-combustion method, which can be easily scaled-up in large quantity at economic cost. This 2D BCNO nanophosphor exhibits a broad highly intense yellow emission peak centered at 580 nm upon 470 nm excitation wavelength with higher quantum efficiency ~89%. The 2D BCNO nanophosphor coated on CoB based blue LEDs device has demonstrated better color coordinates (x = 0.3496, y = 0.3679), lower color temperature (4899 K), better color rendering index (~92), higher luminous efficiency (~83.4 $lmW^{-1}$) and higher brightness (834 $Cd/m^2$). Finally, we envision that this novel rare-earth free 2D light weight BCNO nanophosphor would astonish a new key of success to build up WLED devices that can replace the existing phosphors which can be potentially utilized in next generation WLEDs.

## Notes and references

[a] *CSIR - National Physical Laboratory, Dr K S Krishnan Road, New Delhi, 110012, India*
[b] *Department of Physics, Kalindi College, University of Delhi, New Delhi, 110008, India*

** Corresponding author. Tel.: +91-11-45609385, Fx: +91-11-45609310*
*E-mail address: bipinbhu@yahoo.com*

**† Electronic Supplementary Information (ESI) available: See DOI: 10.1039/b000000x/**

**Acknowledgment**

The authors wish to thank Director, N.P.L., New Delhi, for his keen interest in the work. The authors are thankful to Prof. O. N. Srivastava (Banaras Hindu University, Varanasi) for his encouragement. Mr. Pawan Kumar gratefully acknowledged University Grant Commission (UGC), Govt. of India, for financial assistance under RGNF Research Fellowship, Award No. F1-17.1/2011-12/RGNF-SC-PUN-12604 /(SA-III/Website). The authors are grateful to the CSIR TAPSUN program providing PL instrument facility.

## References:

(1) K. Geim and K. S. Novoselov, *Nat. Mater.*, 2007, **6**, 183−191.
(2) K. S. Novoselov, A. K.Geim, S. V. Morozov, D. Jiang, Y. Zhang, S. V. Dubonos, I. V. Grigorieva and A. A. Firsov, *Science*, 2004, **306**, 666−669.
(3) G**.** Gao, W**.** Gao, E. Cannuccia, J**.** Taha-Tijerina, L**.** Balicas, A**.** Mathkar, T. N. Narayanan, Z**.** Liu, B**.** K. Gupta, J**.** Peng, Y**.** Yin, A**.** Rubio and P**.** M. Ajayan *Nano Lett.*, 2012, **12,** 3518-3525**.**
(4) A. A. Balandin, *Nature Mater.*, 2011, **10**, 569-581.
(5) H. C. Neto, F. Guinea, N. M. R. Peres, K. S. Novoselov and A. K. Geim. *Rev. of Modern Phys.*, 2009, **81**, 109-162.
(6) Y. Kubota, K. Watanabe, O. Tsuda and T. Taniguchi, *Science*, 2007, **317**, 932-934.
(7) K. Watanabe, T. Taniguchi, T. Niiyama, K. Miya and M. Taniguchi, *Nat. Photonics*, 2009, **3**, 591-594.
(8) L. Song, Z. Liu, A. L. M. Reddy, N. T. Narayanan, J. Taha-Tijerina, J. Peng, G. Gao, J. Lou, R. Vajtai and P. M. Ajayan, *Adv. Mater.*, 2012, **24**, 4878-4895.
(9) H. B. Zeng, C. Y. Zhi, Z. H. Zhang, X. L. Wei, X. B. Wang, W. L. Guo, Y. Bando and D. Golberg, *Nano Lett.*, 2010, **10**, 5049-5055.
(10) L. Song, L. J. Ci, H. Lu, P. B. Sorokin, C. H. Jin, J. Ni, A. G. Kvashnin, D. G. Kvashnin, J. Lou, B. I. Yakobson and P. M. Ajayan, *Nano Lett.*, 2010, **10**, 3209-3215.
(11) W. Q. Han, H. G. Yu, C. Zhi, J. Wang, Z. Liu, T. Sekiguchi and Y. Bando, *Nano Lett.*, 2008, **8**, 491-494.
(12) M. G. Silly, P. Jaffrennou, J. Barjon, J. S. Lauret, F. Ducastelle, A. Loiseau, E. Obraztsova, B. Attal-Tretout and E. Rosencher, *Phys. Rev. B*, 2007, **75**, 085205.
(13) D. Portehault, C. Giordano, C. Gervais, I. Senkovska, S. Kaskel, C. Sanchez and M. Antonietti, *Adv. Funct. Mater*., 2010, **20,** 1827-1833.
(14) K. Raidongia, A. Nag, K. P. S. S. Hembram, U. V. Waghmare, R. Datta and C. N. R. Rao, *Chem. Eur. J*., 2010, **16,** 149.
(15) L. W. Yin, Y. Bando, D. Golberg, A. Gloter, M. S. Li, X. L. Yuan and T. Sekiguchi*, J. Am. Chem. Soc.*, 2005, **127**, 16354-16355.
(16) L. Liao, K. H. Liu, W. L. Wang, X. D. Bai, E. G. Wang, Y. L. Liu, J. C. Li and C. Liu, *J. Am. Chem. Soc.*, 2007, **129**, 9562-9563.
(17) J. Yu and E. G. Wang, *Appl. Phys. Lett*., 1999, **74**, 2948.
(18) S. Y. Wang, L. P. Zhang, Z. H. Xia, A. Roy, D. W. Chang, J. B. Baek and L. M. Dai, *Angew. Chem. Int. Ed.*, 2012, **51,** 4209-4212.
(19) H. Konno, T. Ito, M. Ushiro, K. Fushimi and K. Azumi, *J. Power Sources*, 2010, **195,** 1739-1746.
(20) X. Liu, S. Ye, Y. B. Qiao, G. P. Dong, Q. Zhang and J. R. Qiu, *Chem. Commun*., 2009, 4073-4075.
(21) W. W. Lei, D. Portehault, R. Dimova and M. Antonietti, *J. Am. Chem. Soc.*, 2011, **133**, 7121-7127.
(22) J. Dwivedi, P. Kumar, A. Kumar, Sudama, V. N. Singh, B. P. Singh, S. K. Dhawan, V. Shanker and B. K. Gupta, *RSC Adv.*, DOI: 10.1039/C4RA11318G.
(23) Y, Zhang, C. Xie, H. Su, J. Liu, S. Pickering, Y. Wang, W. W. Yu, J. Wang, Y. Wang, J. Hahm, N. Dellas, S. E. Mohney and J. Xu., *Nano Lett.*, 2011, **11**, 329-332.
(24) H. P. T. Nguyen, S. Zhang, A. T. Connie, M. G. Kibria, Q. Wang, I. Shih, and M. Zetian, *Nano Lett.*, 2013, **13**, 5437-5442.
(25) Z.Yang, J. Xu, P. Wang, X. Zhuang, A. Pan and L. Tong, *Nano Lett.*, 2011,**11**, 5085-5089.
(26) W. N. Wang, Y. Kaihatsu, F. Iskandar and K. Okuyama, *Mater. Res. Bull.*, 2009, **22**, 2099-2102.
(27) Y. kaihatsu, W. N. Wang, K. Okuyama, T. Ogi and K. Okuyama, *J. Electrochem. Soc*., 2010, **157**, J329-J333.
(28) T. Ogi, F. Iskandar and A. B. D. Nandiyanto, *J. Chem. Eng. Jpn*., 2012, 45, 995-
(29) T. Ogi, H.. Iwasaki, A. B. D. Nandiyanto, F. Iskandar, W. N. Wang and K. Okuyama, *J. Mater. Chem. C* 2014, **2**, 4297-4303.
(30) T. Ogi, Y. Kaihatsu, F. Iskandar, W. Wang and K. Okuyama, *Adv. Mater.*, 2008, **20**, 3235-3238.
(31) Y. Kaihatsu, F. Iskander, H. Vidyandari W. Wang and K. Okuyama*, Electrochem. Solid state lett.*, 2009, **12,** J33-J36.
(32) A.; Rubio, J. L.; Corkill and M. L. Cohen, *Phys. Rev. B*, 1994, **49**, 5081.
(33) M. S. C. Mazzoni, R. W. Nunes, S. Azevedo and H. Chacham, *Phys. Rev. B*, 2006, **73,** 073108.
(34) M. O. Watanabe, S. Itoh, T. Sasaki and K. Mizushima, *Phys. Rev. Lett*., 1996, **77**, 187.
(35) X. D. Bai, E. G. Wang, J. Yu and H. Yang, *Appl. Phys. Lett*., 2000, **77**, 67.
(36) W. N. Wang, T. Ogi, Y. Kaihatsu, F. Iskandarc and K. Okuyama, *J. Mater. Chem.*, 2011, **21**, 5183-5189.
(37) L. Qin, J. Yu, S. Kuang, C. Xiao and X. Bai, *Nanoscale*, 2012, **4**, 120-123.
(38) G. Kedawat, S. Srivastava, V. K. Jain, P. Kumar, V. Kataria, Y. Agrawal, B. K. Gupta and Y. K. Vijay, *ACS Appl. Mater. Interfaces*, 2013, **5**, 4872-4877.
(39) B. K. Gupta, D. Haranath, S. Saini, V. N. Singh, V. Shanker, *Nanotechnol.*, 2010, **21**, 055607.
(40) K. Mishra, S. K. Singh, A. K. Singh, M. Rai, B. K. Gupta and S. B. Rai, *Inorg Chem*., 2014, **53**, 9561-9569.
(41) G. R. Bhimanapati, D. Kozuch and J. A. Robinson, *Nanoscale*, 2014, **6**, 11671-11675.
(42) P. Thanikaivelan, T. N. Narayanan, L. Song, W. Gao, T. Hayashi, A. L. M. Reddy, A. Saha, V. Shanker, M. Endo, A. A. Marti and P. M. Ajayan, *Nano Lett.*, 2011, **11**, 5227-5233.
(43) M. Hubacek, T. Sato and T. Ishii, *J. Solid State Chem.*, 1994, **109**, 384-390.
(44) V. Brozek and M. Hubacek*, J. Solid State Chem.*, 1992, **100**, 120-129.
(45) M. A. Mannan, M. Nagano, K. Shigezumi, T. Kida, N. Hirao and Y. Baba, *Am. J. Appl. Sci.*, 2008, **5**, 736-741.
(46) C. C. Tang, Y. Bando, C. Y. Zhi and D. Golberg, *Chem. Commun*., 2007, **44**, 4599-4601.
(47) X. Zhang, Z. Lu, J. Lin, L. Li, Y. Fan, L. Hu, X. Xu, F. Meng, J. Zhao and C. Tang, *Mater. Lett*., 2013, **94**, 72-75.